

# Small Signal Audiosusceptibility Model for Series Resonant Converter

Subhash Joshi T.G.  
Member, IEEE

Power Electronics Group  
Centre for Development of Advanced Computing  
Thiruvananthapuram-695033, India  
Email:subhashj@cdac.in

Vinod John

Senior Member, IEEE  
Department of Electrical Engineering  
Indian Institute of Science  
Bangalore-560012, India  
Email:vjohn@iisc.ac.in

**Abstract**—Models that accurately predict the output voltage ripple magnitude are essential for applications with stringent performance target for it. Impact of dc input ripple on the output ripple for a Series Resonant Converter (SRC) using discrete domain exact discretization modelling method is analysed in this paper. A novel discrete state space model along with a small signal model for SRC considering 3 state variables is presented. The audiosusceptibility (AS) transfer function which relates the input to output ripple is derived from the small signal model. Analysis of the AS transfer function indicates a resonance peak and an expression is derived connecting the AS resonance frequency for input ripple with different SRC component values. Further analysis is done to show that a set of values for SRC parameter exists, which forms a design region, for which the normalized gain offered by the SRC for input ripple is less than unity at any input ripple frequency. A test setup to introduce the variable frequency ripple at the input of SRC for the experimental evaluation of AS transfer function is also proposed. Influence of stray parameters on AS gain, AS resonance frequency and on SRC tank resonance frequency is addressed. An SRC is designed at a power level of  $10kW$ . The analysis using the derived model, simulations, and experimental results are found to be closely matching.

**Index Terms**—series resonant converter, sampled data modelling, audiosusceptibility, small signal model

## I. INTRODUCTION

Series Resonant Converter (SRC), shown in Fig. 1, is the preferred topology for High Voltage (HV) low current power supply due to the absence of magnetics at the HV side [1]. Radar, X-rays are some of the applications where such HV power supplies are used. Some of these applications impose stringent performance parameters on the HV power supply such as voltage ripple and regulation [2]. To maintain better imaging quality for radar and X-ray image contrast, these applications demand a good control over dc voltage ripple of less than 0.001%. In this paper an analysis is carried out to evaluate the contribution of input voltage ripple on output voltage ripple, which is also referred to as audiosusceptibility (AS) model [3].

Small signal models of resonant converters are of interest over a long time and recent works have further refined the converter model [4]–[11]. In many small signal models, transfer functions are derived based on numerical solutions instead of analytical solutions that result in loss of physical insight,

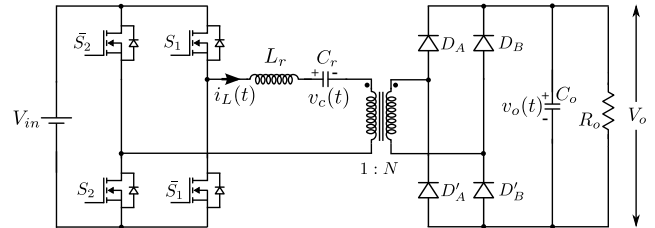


Fig. 1. SRC showing the state variables.

which hampers its use for design purpose. The widely used state-space averaging approach fails for resonant converter since the states are of ac behaviour [4]. Small signal models for SRC are derived by using High-Q approximation [5]. Another modelling approach is by the low frequency approximation of the states [6]. Both these approaches have sinusoidal waveform assumption that results in accuracy limitations. The small signal transfer functions of SRC in [7] are derived numerically due to the difficulty in converting it into an analytical expression form. In [8] the amplitude and the phase of the states are transformed into slowly varying signals where the accuracy is improved by finding a series of averaged models which necessitate the use of numerical approach. In extended describing function method each non-linear elements are approximated by its first harmonic sinusoids [9], [10]. In contrast, the discrete domain modelling method using exact discretization, that is also referred as sampled data modelling method, can be employed without any approximation and hence it is capable of analysing the circuit accurately [11]. In this method the modelling is carried out by solving time segmented piece-wise linear time invariant state equations by use of the switching boundary conditions. Then by performing the perturbation and linearisation, a small signal model is accurately obtained. Due to the analysis complexity, the converter models using exact discretization modelling method reported so far only provide numerical solutions [12].

In [13], the state space model of the SRC over a switching period is obtained analytically by using exact discretization modelling approach. A simple method to handle the resonant tank and output filter state variables of the SRC while for-

mulating the combined state space equation for the switching period  $T_s$  has been proposed. From the state space model of SRC, an analytical expression for small signal model connecting the input and states is derived. The audiosusceptibility (AS) transfer function is also derived from the small signal model. The resulting model provides analytical parameter relationships and physical insights into the system in terms of SRC circuit parameters.

In this paper it is shown that it is possible to have a resonance peak in the AS transfer function of the SRC. An analytical expression is derived for the AS resonance frequency for input ripple and its relationship with different SRC components is shown. It is also demonstrated that the AS resonance frequency is much lower than the SRC tank resonance frequency which is decided by the resonant tank components. From the derived transfer function, the paper discusses the gain and open-loop bandwidth offered by the SRC to variations in input frequency. The frequency response to input ripple is verified by simulations and compared with the derived analytical expressions for different values of effective quality factor,  $Q_e$ , and ratio of switching frequency to SRC tank resonance frequency,  $F$ , where  $Q_e$  is as defined in [14]. The paper extends the analysis to show that a set of value for  $F$  and  $Q_e$  exists for which the normalized gain offered by SRC for input ripple is less than unity for any input ripple frequency. The paper utilizes this finding to identify a design and operating region that relate  $Q_e$  and  $F$  with the “less than unity gain” in audiosusceptibility. This region derived from the analytical AS transfer function is verified by time domain simulation results. An SRC is designed at a power level of  $10kW$ . An operating condition is chosen to demonstrate the AS resonance for input ripple. The paper also proposes a test setup to introduce variable frequency ripple at the input of the SRC for the experimental evaluation of AS transfer function. The influence of stray parasitic parameters on AS gain, AS resonance frequency, and on SRC tank resonance frequency are verified by the model, simulation and experiment. It is shown that the influence of stray parameter on AS resonance frequency is minimal. The analysis of the derived model, simulation and experimental results are found to be closely matching.

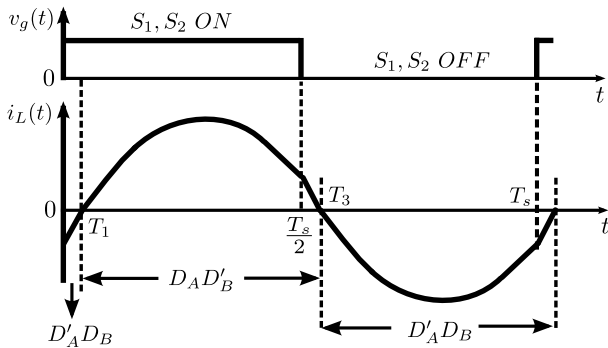


Fig. 2. Switching sequence of SRC.

TABLE I  
NOMINAL VALUES OF SRC PARAMETERS

Parameters	Values
DC input voltage ( $V_{in}$ )	700V
DC input ripple frequency	100Hz – 10kHz
Output power	10kW
DC output voltage ( $V_o$ )	10kV
DC output voltage ripple	0.1%
SRC resonance frequency	100kHz
Range of $F$	1.01 – 1.5
Range of $Q_e$	0.5 – 10

## II. DISCRETE STATE SPACE MODEL OF SRC

The SRC circuit with the labelled components are shown in Fig. 1. The state variables chosen are resonant capacitor ( $C_r$ ) voltage  $v_c(t)$ , resonant inductor ( $L_r$ ) current  $i_L(t)$  and output capacitor ( $C_o$ ) voltage  $v_o(t)$ . Turning ON of switch  $S_1$  and  $S_2$  at  $t = 0$  indicates the starting of first switch configuration in the operation of SRC out of the four switch configurations present in  $T_s$  shown in Fig. 2. First switch configuration ends and second switch configuration starts when  $i_L(t)$  reaches zero from negative polarity at time  $T_1$ . When switch  $S_1$  and  $S_2$  are turned OFF at time  $T_s/2$  second switch configuration ends and third switch configuration starts [2]. Third switch configuration ends at time  $T_3$  when  $i_L(t)$  reaches zero from positive polarity and fourth switch configuration continues until  $S_1$  and  $S_2$  are again turned ON. The range of input ripple frequency  $f_{in}$  is chosen from 100Hz to 10kHz. The operating frequency of SRC,  $f_s$ , considered in the analysis is above its tank resonance frequency and are in the range of 100kHz. Table I gives the values of various SRC parameters considered for the time domain simulation for verifying the analysis.

### A. Exact discretization

In this analysis the state space model of the SRC is derived using exact discretization modelling [15]. It is assumed that the states of the system are represented by linear time invariant differential equations and the state variable values are continuous from one switch configuration to the next. Hence the states at the end of one switch configuration form the initial condition for the next switch configuration. If  $x[kT_s]$  is the initial condition of the state at  $k^{th}$  sample and  $u(t)$  is the input between  $k^{th}$  sample and time  $kT_s + t$ , then states at  $kT_s + t$  is,

$$x[kT_s + t] = e^{A([kT_s + t] - kT_s)} x[kT_s] + \int_{kT_s}^{kT_s + t} e^{A([kT_s + t] - \tau)} B u(\tau) d\tau \quad (1)$$

where,  $A$ ,  $B$  are the state matrices derived from dynamic equations valid between  $kT_s$  and  $kT_s + t$  [15]. Initial conditions of the states  $x[kT_s] = [I_L \ V_c \ V_o]^T$ , where  $I_L$ ,  $V_c$  and  $V_o$  are the values of the states at time  $t = kT_s$ . The input to the SRC

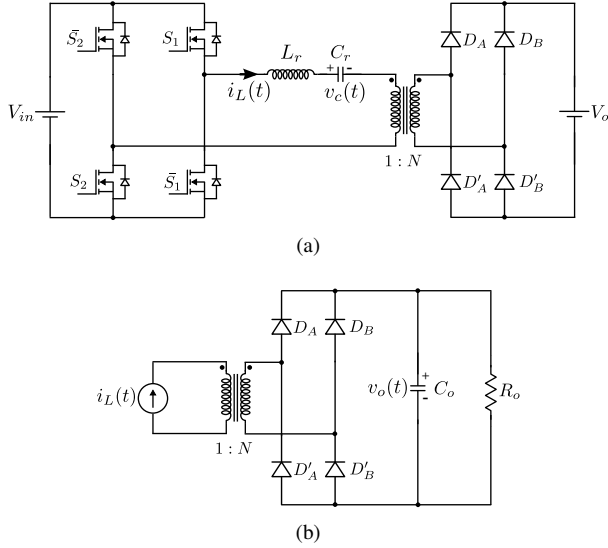


Fig. 3. Equivalent circuit diagram with (a) constant dc output (b) input modelled as current source.

at  $t = kT_s$  is  $u[kT_s] = [V_{in}]$ . The term  $e^{At}$  is computed by evaluating  $L^{-1}([sI - A]^{-1})$ .

### B. Non-linear state equations of SRC

The state equations of SRC are formulated with 3 state variables for the analysis of audiosusceptibility. This is carried out in two steps by using 2 plus 1 state variable approach. In *Step 1*, 2 state variables and in *Step 2* remaining one state variable are considered.

1) *Step 1*: Since the range of  $f_{in}$  of interest is an order less than  $f_s$ , the variation in  $v_{in}(t)$  and  $v_o(t)$  at frequency  $f_{in}$  are neglected in a switching period  $T_s$ . This simplifies the analysis to 2 state variables as shown in Fig. 3(a).  $x(t) = [i_L(t) v_c(t)]^T$  with input  $u(t) = [V_{in} V_o]^T$  is evaluated and the state variable  $[v_o(t)]$  is evaluated subsequently. The dynamic equations from the simplified equivalent diagram shown in Fig. 3(a) gives the state matrices related to the four switch configurations represented by suffix from 1 to 4 given by,

$$A_1=A_2=A_3=A_4 = \begin{bmatrix} 0 & -\frac{1}{L_r} \\ \frac{1}{C_r} & 0 \end{bmatrix}, B_1 = -B_3 = \begin{bmatrix} \frac{1}{L_r} & \frac{1}{NL_r} \\ 0 & 0 \end{bmatrix} \quad (2)$$

$$B_2 = -B_4 = \begin{bmatrix} \frac{1}{L_r} & -\frac{1}{NL_r} \\ 0 & 0 \end{bmatrix}$$

Substituting  $(A_1, B_1)$  from (2) and input  $u(t) = [V_{in} V_o]^T$  in (1), the state at the end of first switch configuration  $x[kT_s + T_1]$  at  $t = T_1$  is derived which is the initial condition for the second switch configuration. The state at the end of second switch configuration  $x[kT_s + (T_s/2)]$  is derived using the state matrices  $(A_2, B_2)$  given in (2) and the same input

$u(t)$ . This procedure is continued until the states at the end of switching period  $x[kT_s + T_s]$  are derived.

$$x[kT_s + T_s] = \begin{bmatrix} \mathbf{a}_{11} & \mathbf{a}_{12} \\ \mathbf{a}_{21} & \mathbf{a}_{22} \end{bmatrix} x[kT_s] + \begin{bmatrix} \mathbf{a}_{13} & \mathbf{b}_{11} \\ \mathbf{a}_{23} & \mathbf{b}_{21} \end{bmatrix} u[kT_s] \quad (3)$$

$$\text{where } x[kT_s] = [I_L \ V_c]^T, \quad u[kT_s] = [V_o \ V_{in}]^T$$

The elements  $\mathbf{a}_{13}$  and  $\mathbf{a}_{23}$  are defined as in (3) to aid the development of the state space model of the overall system as explained in section II-C. The elements in the matrices are given in Appendix A.1.

2) *Step 2*:  $v_o(t)$  is determined by the current  $i_L(t)$ . Hence,  $i_L(t)$  is considered as an input current source for the estimation of the state variable  $v_o(t)$  for the period  $T_s$  where  $i_L(t)$  is updated in *Step 1* in each  $T_s$ . This simplifies the circuit to one state variable  $x(t) = [v_o(t)]$  and input  $u(t) = [i_L(t)]$ . The state matrices related to four switch configurations represented by suffix from 1 to 4 are obtained using the dynamic equations from the simplified equivalent diagram shown in Fig. 3(b).

$$A'_1=A'_2=A'_3=A'_4 = \begin{bmatrix} -\frac{1}{R_o C_o} \end{bmatrix}, \quad (4)$$

$$B'_1 = -B'_2 = -B'_3 = B'_4 = \begin{bmatrix} -\frac{1}{NC_o} \end{bmatrix}$$

The input  $u(t)$  for each switch configuration can be found from the solution of the state  $i_L(t)$  for each switch configuration derived in *Step 1*. Substituting  $(A', B')$  matrices given in (4) and  $u(t)$  obtained from *Step 1* in (1), the states for each switch configuration are derived. Using the state at the end of each switch configuration as an initial condition for the next switch configuration, the state at the end of  $T_s$  is given by,

$$x[kT_s + T_s] = [\mathbf{a}_{33}] x[kT_s] + [\mathbf{a}_{31} \ \mathbf{a}_{32} \ \mathbf{b}_{31}] u[kT_s] \quad (5)$$

$$\text{where } x[kT_s] = [V_o], \quad u[kT_s] = [I_L \ V_c \ V_{in}]^T$$

The elements in the matrices of (5) are given in Appendix A.2. Even though the input  $u(t) = [i_L(t)]$ , the waveform for  $i_L(t)$  also depends on the initial conditions of  $v_c(t)$  and  $v_{in}(t)$ . Hence, this results in  $u[kT_s] = [I_L \ V_c \ V_{in}]^T$  as expressed in (5).

### C. Discrete state space model of SRC

The discrete domain state space model is obtained by combining the 2 state variables model in *step1* and 1 state variable model in *step2* given in (3) and (5) respectively. This yields the complete discrete domain state space model of the SRC.

$$x[kT_s + T_s] = A_d x[kT_s] + B_d u[kT_s] \quad (6)$$

$$A_d = \begin{bmatrix} \mathbf{a}_{11} & \mathbf{a}_{12} & \mathbf{a}_{13} \\ \mathbf{a}_{21} & \mathbf{a}_{22} & \mathbf{a}_{23} \\ \mathbf{a}_{31} & \mathbf{a}_{32} & \mathbf{a}_{33} \end{bmatrix}, \quad B_d = \begin{bmatrix} \mathbf{b}_{11} \\ \mathbf{b}_{21} \\ \mathbf{b}_{31} \end{bmatrix}, \quad (7)$$

$$x[kT_s] = [I_L \ V_c \ V_o]^T, \quad u[kT_s] = [V_{in}]$$

Using (6) the SRC is described by the states, input and the time durations as shown in Fig. 2. Hence (6) can be described by,

$$x[kT_s + T_s] = f(x, u, T_s, T_1, T_3) \quad (8)$$

This is a state space model of a discrete-time non-linear system. It can be linearized after identifying the equilibrium operating trajectory for the system.

### III. SMALL SIGNAL MODEL OF SRC

The steady state waveforms of the SRC are periodic with period  $T_s$ . The steady state values of the  $x[kT_s]$  are derived as follows.

#### A. Cyclic steady state model of SRC

The cyclic steady state variables of the SRC is denoted by the superscript  $s$  if (9) and (10) are satisfied [15].

$$x^s[kT_s + T_s] = f(x^s, u^s, T_s, T_1^s, T_3^s) = x^s[kT_s] \quad (9)$$

$$i_L^s(kT_s + T_1) = 0, \quad i_L^s(kT_s + T_3) = 0, \quad (10)$$

Equation (9) represents the cyclic steady state condition of the states and (10) represents the constraint for times  $T_1$  and  $T_3$ . Substituting the state equation for  $i_L(t)$  from (6) in (10), the cyclic steady state time  $T_1^s$  and  $T_3^s$  is constrained by (11) and (12).

$$f_{T1} = I_L^s \cos \omega_r T_1^s - \frac{V_c^s - V_{in}^s - \frac{V_o^s}{N}}{Z_c} \sin \omega_r T_1^s = 0 \quad (11)$$

$$f_{T3} = I_L^s \cos \omega_r T_3^s - \frac{V_c^s - V_{in}^s - \frac{V_o^s}{N}}{Z_c} \sin \omega_r T_3^s - \quad (12)$$

$$\frac{2V_o^s}{NZ_c} \sin \omega_r (T_3^s - T_1^s) - \frac{2V_{in}^s}{Z_c} \sin \omega_r (T_3^s - \frac{T_s}{2}) = 0$$

#### B. Small signal model of SRC

Since the small signal analysis is restricted to audiosusceptibility the switching period  $T_s$  of SRC is held constant and a small variation for the input is applied about the cyclic steady state. This resulting variations are denoted by the symbol  $\tilde{\cdot}$  in the states, input, and subinterval times and are given by (13).

$$\begin{aligned} \tilde{i}_L[kT_s] &= I_L[kT_s] - I_L^s[kT_s], \\ \tilde{v}_c[kT_s] &= V_c[kT_s] - V_c^s[kT_s], \\ \tilde{v}_o[kT_s] &= V_o[kT_s] - V_o^s[kT_s], \\ \tilde{v}_{in}[kT_s] &= V_{in}[kT_s] - V_{in}^s[kT_s], \\ \tilde{t}_{1,k} &= T_{1,k} - T_{1,k}^s, \quad \tilde{t}_{3,k} = T_{3,k} - T_{3,k}^s \end{aligned} \quad (13)$$

where,  $T_{1,k}$  and  $T_{3,k}$  are the values of  $T_1$  and  $T_3$  during the  $k^{th}$  sample.

By substituting (13) in (6) the variation in states at  $kT_s + T_s$  is,

$$\tilde{x}[kT_s + T_s] = x[kT_s + T_s] - x^s[kT_s + T_s] \quad (14)$$

Applying the Taylor series expansion at the steady-state operating point in (8) and truncating the higher order non-linear terms gives the linearized small signal model as,

$$\tilde{x}[kT_s + T_s] = \left. \frac{\partial f}{\partial x} \right|_{x^s} \tilde{x} + \left. \frac{\partial f}{\partial u} \right|_{u^s} \tilde{u} + \left. \frac{\partial f}{\partial T_1} \right|_{T_1^s} \tilde{t}_1 + \left. \frac{\partial f}{\partial T_3} \right|_{T_3^s} \tilde{t}_3 \quad (15)$$

Since the elements of matrices  $A_d$  and  $B_d$  are functions of time  $T_1$  and  $T_3$ , substituting (6) in (15) gives,

$$\tilde{x}[kT_s + T_s] = A_d \tilde{x}[kT_s] + B_d \tilde{u}[kT_s] + T_d \tilde{t}_k \quad (16)$$

where,

$$\begin{aligned} T_d &= \begin{bmatrix} \left[ \frac{\partial A_d}{\partial T_1} \frac{\partial B_d}{\partial T_1} \right] & \left[ \frac{\partial A_d}{\partial T_3} \frac{\partial B_d}{\partial T_3} \right] \\ \left[ \frac{\partial A_d}{\partial T_1} \frac{\partial B_d}{\partial T_1} \right] & \left[ \frac{\partial A_d}{\partial T_3} \frac{\partial B_d}{\partial T_3} \right] \end{bmatrix} \begin{bmatrix} x[kT_s] \\ u[kT_s] \end{bmatrix}, \\ \tilde{x}[kT_s] &= \begin{bmatrix} \tilde{i}_L \\ \tilde{v}_c \\ \tilde{v}_o \end{bmatrix}, \quad \tilde{u}[kT_s] = [\tilde{v}_{in}], \quad \tilde{t}_k = \begin{bmatrix} \tilde{t}_1 \\ \tilde{t}_3 \end{bmatrix} \end{aligned} \quad (17)$$

The order of  $T_d$  is  $3 \times 2$  where the columns are obtained by the product of two matrices of the order  $3 \times 4$  and  $4 \times 1$ . Using (7) in the expression for  $T_d$  in (17), the elements  $\text{td}_{pq}$  of  $T_d$ , where suffix  $(p, q)$  represent the row and column indices, are tabulated in Appendix A.3.

1) *Estimation of  $\tilde{t}_k$* : Expanding the dynamics constraint in (11) and (12) by using Taylor series expansion and truncating the higher order non-linear terms gives,

$$\tilde{f}_{T1} = \left. \frac{\partial f_{T1}}{\partial x} \right|_{x^s} \tilde{x} + \left. \frac{\partial f_{T1}}{\partial u} \right|_{u^s} \tilde{u} + \left. \frac{\partial f_{T1}}{\partial T_1} \right|_{T_1^s} \tilde{t}_1 + \left. \frac{\partial f_{T1}}{\partial T_3} \right|_{T_3^s} \tilde{t}_3 = 0 \quad (18)$$

$$\tilde{f}_{T3} = \left. \frac{\partial f_{T3}}{\partial x} \right|_{x^s} \tilde{x} + \left. \frac{\partial f_{T3}}{\partial u} \right|_{u^s} \tilde{u} + \left. \frac{\partial f_{T3}}{\partial T_1} \right|_{T_1^s} \tilde{t}_1 + \left. \frac{\partial f_{T3}}{\partial T_3} \right|_{T_3^s} \tilde{t}_3 = 0 \quad (19)$$

By solving (11) and (12),  $\tilde{t}_1$  and  $\tilde{t}_3$  can be represented in terms of  $\tilde{x}$  and  $\tilde{u}$  as,

$$\tilde{t}_k = T_{kx} \tilde{x}[kT_s] + T_{ku} \tilde{u}[kT_s] \quad (20)$$

The elements of  $T_{kx}$  and  $T_{ku}$  are denoted by  $\text{tx}_{pq}$  and  $\text{tu}_{pq}$  respectively where the suffix represents the row and column numbers. These elements are given in Appendix A.4. Substituting (20) in (16) gives the overall small signal model of SRC in terms of states and input and is given by,

$$\begin{aligned} \tilde{x}[kT_s + T_s] &= A_{sd} \tilde{x}[kT_s] + B_{sd} \tilde{u}[kT_s] \\ \text{where } A_{sd} &= [A_d + T_d T_{kx}] \quad B_{sd} = [B_d + T_d T_{ku}] \end{aligned} \quad (21)$$

This represents a system with states representing the incremental components of resonant capacitor voltage, resonant inductor current and output voltage at the discrete time sampling time instants. The input for this model is the incremental input voltage,  $\tilde{v}_{in}[kT_s]$ .

#### C. Simplified small signal model of SRC

The dynamic model in (21) can be used to obtain the relationships between the input voltage  $\tilde{v}_{in}[kT_s]$  and the state variables  $\tilde{x}[kT_s]$  with the coefficients of the dynamic system matrices given in the Appendix. However, it is possible to simplify the entries of the matrices by making some practical assumptions.

The major assumption made for simplifying the small signal model is  $T_3 = (T_s/2) + T_1$ . Additional practical assumptions made are  $e^{\frac{t}{R_o C_o}} \approx 1, \forall 0 \leq t \leq T_s$  and  $\frac{1}{(R_o C_o)^2} \ll \omega_r^2$ . This implies that the output voltage decay is neglected over a switching period, and the reciprocal of the output time constant is much lower than the tank resonance frequency.

These simplify the  $A, B$  matrices of the small signal model as,

$$\bar{A}_{sd} = \begin{bmatrix} 1 + \frac{4\omega_r V_o}{NZ_c f'_{T1}} & -\frac{\sin \omega_r T_s}{Z_c} & 0 \\ Z_c \sin \omega_r T_s & 1 & \frac{4}{N} \\ 0 & -\frac{4}{NZ_c C_o \omega_r} & 1 \end{bmatrix}, \bar{B}_{sd} = \begin{bmatrix} 0 \\ -4 \\ 0 \end{bmatrix} \quad (22)$$

Small signal input to output transfer functions in the z-domain are found by substituting (22) in (21). The obtained audiosusceptibility transfer function in z-domain is given in (23) where  $f'_{T1} = -df_{T1}/dt$ . The complex roots of denominator shows a resonance in the frequency response and the possibility of high gain of the SRC for input ripple. The s-domain AS resonance frequency for input ripple is obtained from the complex roots of denominator polynomial and is given by,

$$\omega_{in,r} = \frac{1}{T_s} \tan^{-1} \left( \sqrt{\frac{16}{N^2 C_o \omega_r Z_c}} \right) \quad (24)$$

The small signal analytical model for audiosusceptibility of a SRC given in (23) is compared with the time domain simulations and experimental results to verify the analytical model.

#### IV. SIMULATION RESULTS

Conventionally, SRC design is based on two quantities (i)  $F$  defined as the ratio of switching frequency  $f_s$  to tank resonance frequency  $f_r$  of SRC (ii)  $Q_e$  defined as the effective quality factor of SRC [14]. Hence to cover a wide range of SRC design, analysis is carried out based on  $F$  and  $Q_e$  where  $F \in [1.01, 1.5]$  and  $Q_e \in [0.5, 10]$ . Time domain simulations are carried out for the validation of model in (23) where normalized gain is defined as,

$$Gain_{\%R} = \frac{|\tilde{v}_0/\tilde{v}_{in}|}{|V_0/V_{in}|} \quad (25)$$

In Figs. 4(a) and (b) the input ripple frequency is varied from  $100Hz$  to  $10kHz$  keeping the quality factor  $Q_e=0.5$  and  $Q_e=2.0$  respectively. At each frequency the gain,  $Gain_{\%R}$ , is computed from (25) for different values of  $F \in [1.01, 1.5]$ . In both Figs. 4(a) and (b), the peak  $Gain_{\%R}$  reduces as  $F$  increases. Also from Fig. 4(a) the maximum  $Gain_{\%R}$  is 23 which occurs at  $\omega_{in,r(s)}$  of  $3950Hz$  for  $F = 1.01$ . The decrease in  $Gain_{\%R}$  for higher  $F$  is found to be consistent for other  $Q_e \in [0.5, 10]$ . Figs. 5(a) and (b) shows  $Gain_{\%R}$  for  $f_{in}$  varied from  $100Hz$  to  $10kHz$  keeping  $F = 1.01$  and  $F = 1.05$  respectively. The  $Gain_{\%R}$  reduces as  $Q_e$  increases in both Figs. 5(a) and (b). The decrease in  $Gain_{\%R}$  for higher  $Q_e$  is also found to be consistent for other  $F \in [1.01, 1.5]$ .

The gain plot from simulation and analytical model in (23) are compared in Figs. 6(a) and (b) for  $Q_e$  and  $F$  of (2,1.01) and (3,1.05) respectively. In these gain plots the gain is defined as,

$$Ripple\ gain = 20 \log_{10} (|\tilde{v}_o/\tilde{v}_{in}|) \text{ dB} \quad (26)$$

The Figs. 6(a) and (b) show that the simulation and the analytical models are closely matching.

$\omega_{in,r}$  and  $\omega_{in,r(s)}$  are the frequencies at which AS resonance occurs in the small signal analytical model and in the time domain simulation respectively. Let the error in the frequency be defined as,

$$\Delta\omega_{in,r\%} = \frac{\omega_{in,r(s)} - \omega_{in,r}}{\omega_{in,r(s)}} 100 \quad (27)$$

The  $\Delta\omega_{in,r\%}$  computed for  $F=1.01$ ,  $F=1.03$  and  $Q_e \in [0.5, 10]$  is shown in Fig. 7(a). Similar results are shown for  $F=1.03$ ,  $F=1.1$  and  $Q_e \in [0.5, 10]$  in Fig. 7(b). Maximum error  $\Delta\omega_{in,r\%}$  is found to be within  $\pm 4\%$  which indicate good match of the analytical audiosusceptibility resonance frequency prediction with simulation results.

#### A. SRC design for superior audiosusceptibility

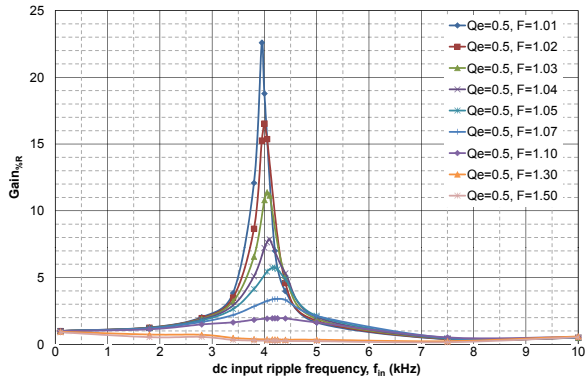
Each curve in Figs. 4(a) and (b) and Figs. 5(a) and (b) represents an SRC design with appropriated  $F$  and  $Q_e$  parameters. From the plots it is seen that there exists a set of values for  $F$  and  $Q_e$  where audiosusceptibility gain of the SRC is always less than unity for any  $f_{in}$ . Such values are identified and plotted as a region above the curves shown in Fig. 8. Such a region obtained based on the analytical model using the gain expression in (23) and that using simulations are also compared in Fig. 8. Design of the SRC using  $F$  and  $Q_e$  values from this region is advantageous as it will have reduced audiosusceptibility with inherent ability to reject disturbance in the input voltage,  $V_{in}$ .

#### V. EXPERIMENTAL RESULTS

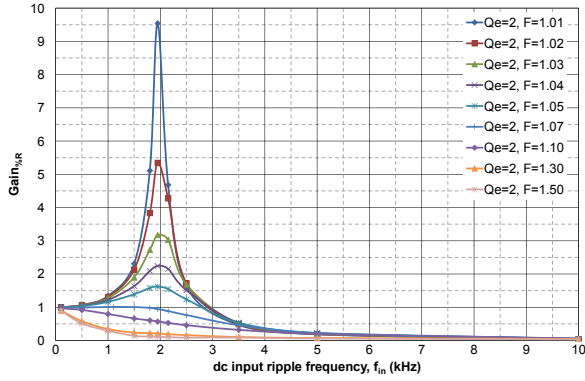
##### A. Test setup

The test setup shown in Fig. 9(a) is used to validate the audiosusceptibility response of the SRC. This setup consists of two H-bridge inverters and an SRC. The H-bridge is built using an IGBT, shown in Fig. 9(b). The inductors  $L_{inv1}$  and  $L_{inv2}$  act as a load for H-bridge1 and H-bridge2 respectively. The objective of the H-bridge inverters are to introduce a known frequency of ripple in the dc voltage  $V_{in}$  at the input of SRC. This is achieved by modulating the switches of the H-bridge with unipolar PWM, where the gate signals are generated by comparing the triangle carrier with sinusoidal modulating signal. The switching frequency of H-bridge is

$$\frac{v_o(z)}{v_{in}(z)} = \frac{\frac{16}{NZ_c C_o \omega_r} \left\{ (z-1) - \frac{4V_o}{NZ_c f'_{T1}} \right\}}{(z-1)^3 - \frac{4V_o}{NZ_c f'_{T1}} (z-1)^2 + \frac{16}{N^2 Z_c C_o \omega_r} (z-1) - \frac{64V_o}{N^3 Z_c^2 C_o \omega_r f'_{T1}}} \quad (23)$$

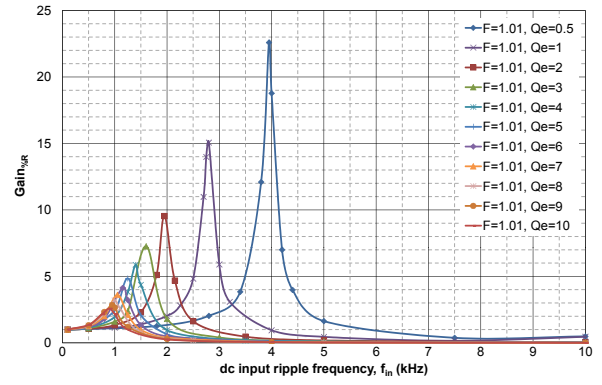


(a)

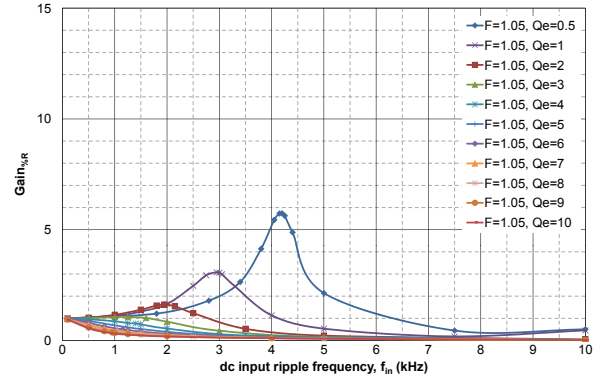


(b)

Fig. 4. Gain versus  $f_{in}$  from simulation for  $F \in [1.01, 1.5]$  and (a)  $Q_e = 0.5$  (b)  $Q_e = 2.0$ .



(a)



(b)

Fig. 5. Gain versus  $f_{in}$  from simulation for  $Q_e \in [0.5, 10]$  and (a)  $F = 1.01$  (b)  $F = 1.05$ .

TABLE II

VALUES OF COMPONENTS USED IN THE AUDIOSUSCEPTIBILITY TEST CIRCUIT

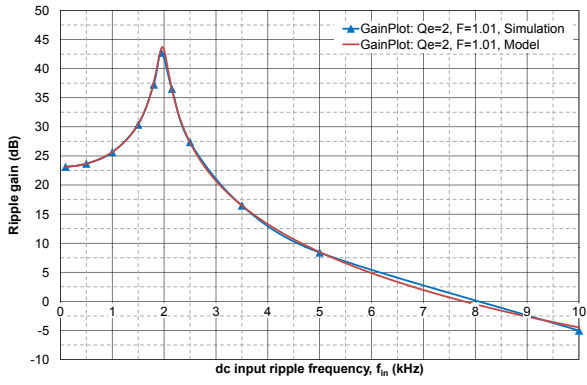
Parameters	Values
$L_{in}$	20mH
$C_{in}$	900 $\mu$ F
$L_{inv1}, L_{inv2}$	0.165mH
Resonant inductor, $L_r$	150 $\mu$ H
Resonant capacitor, $C_r$	16nF
Output filter capacitor, $C_o$	100nF
Load resistance, $R_o$	10k $\Omega$
Turns ratio of transformer, $N$	16
Leakage inductance of transformer referred to primary	15 $\mu$ H
Stray capacitance of transformer referred to primary, $C_s$	2.85nF

chosen as 10kHz and unipolar PWM pushes the effective switching frequency to 20kHz. H-bridge2, is also modulated as that of H-bridge1 except the carrier of H-bridge2 is shifted by 90° from the carrier of H-bridge1 as shown in Fig. 9(c). Such a phase shift pushes the effective switching frequency to 40kHz, which is twice the individual H-bridge effective switching frequency.

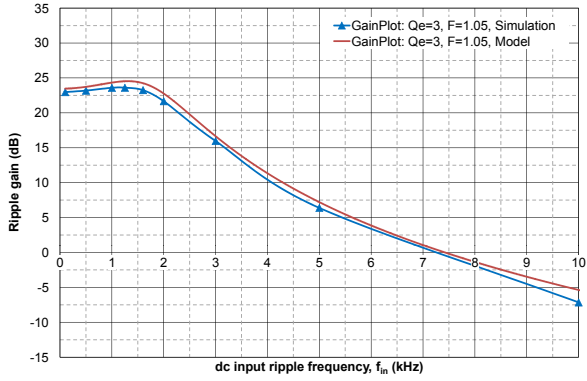
For the audiosusceptibility test of SRC, the ripple frequency in  $V_{in}$  is varied between 100Hz and 4kHz. Hence the current

drawn from the capacitor  $C_{in}$  by H-bridge1 and H-bridge2, referred to as  $i_{dc1}$  and  $i_{dc2}$  respectively, should be of frequency between 100Hz and 4kHz. This is achieved by choosing the frequency of modulating signal between 50Hz and 2kHz, which is also equal to the frequency of inverter current  $i_{inv1}$  and  $i_{inv2}$  shown in Fig. 9(a). The higher value of effective switching frequency of 40kHz allows one to achieve a high ripple frequency of 4kHz with reduced unwanted frequencies. The inductor  $L_{in}$  shown in Fig. 9(a) connected in series with the variable dc source  $V_{dc}$  ensures that ripple of frequency between 100Hz and 4kHz in  $i_{dc1}$  and  $i_{dc2}$  are primarily drawn only from the dc capacitor  $C_{in}$ . The corner frequency chosen for  $L_{in}$  and  $C_{in}$  is 37.5Hz. The values of  $L_{inv1}$  and  $L_{inv2}$  are chosen to give an appreciable ripple in  $V_{in}$ . The SRC is designed for an output voltage of 10kVdc for an input voltage of 625Vdc and nominal output power of 10kW. The tank resonance frequency contributed by  $L_r$  and  $C_r$  is chosen as 102kHz. The values of various components used in the H-bridge inverters and SRC are given in Table II. Even though the rated input voltage of the SRC is 625Vdc, the audiosusceptibility test is carried out at a low input voltage around 10Vdc, considering that AS resonance conditions may be excited.

After turning on the SRC, the H-bridge1 and H-bridge2 are turned on to introduce a ripple in  $V_{in}$ . The frequency



(a)



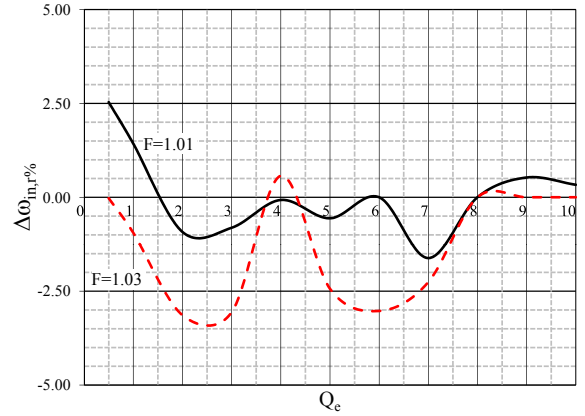
(b)

Fig. 6. Comparison of small signal model with simulation for frequency response when (a)  $Q_e = 2$  and  $F = 1.01$  (b)  $Q_e = 3$  and  $F = 1.05$ .

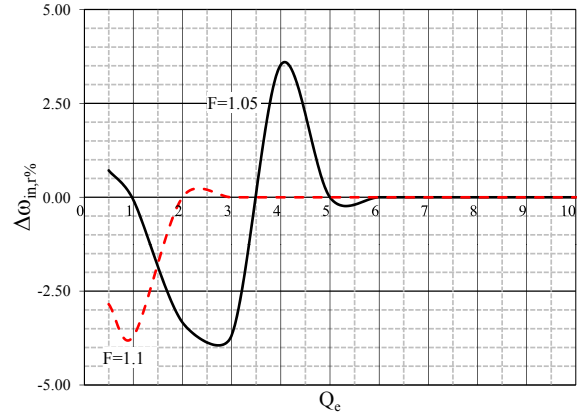
of the modulating signal is varied from  $50\text{Hz}$  to  $2\text{kHz}$ , incremented in a step of  $50\text{Hz}$ . At each step, the ripple in input  $V_{in}$  and output  $V_o$  is recorded with an oscilloscope of  $5\text{Gs/s}$  sampling rate. The built-in spectrum analysis function of the oscilloscope is used to find the magnitude and frequency spectrum of the sensed signal  $V_{in}$  and  $V_o$ . By measuring the dc gain of SRC and from the measured magnitude of ripple in  $V_{in}$  and  $V_o$  the audiosusceptibility gain is computed by (25). The audiosusceptibility gain is plotted for each ripple frequency to find the SRC frequency response to input ripple.

### B. Estimation of SRC tank resonance frequency ( $f_r$ )

Even though the values of  $L_r$  and  $C_r$  are chosen for a tank resonance frequency of  $102\text{kHz}$ , due to the presence of magnetizing inductance and stray capacitance of the transformer the effective tank resonance frequency will be different from  $102\text{kHz}$ . An impulse signal is applied across  $M_1$  and  $M_2$  referred in Fig. 9(a) to estimate the actual SRC tank resonance frequency. The experiment is conducted along with the dc side load  $R_o$ . The impulse signal is generated with the same test setup shown in Fig. 9(a). The H-bridge inverters are kept in the off condition and the switches of SRC are triggered appropriately to generate an impulse voltage of  $10\mu\text{s}$  duration across  $M_1$  and  $M_2$ . The frequency of the resonant inductor current  $i_L(t)$  is measured to compute the tank resonance



(a)



(b)

Fig. 7.  $\Delta\omega_{in,r}\%$  for  $Q_e \in [0.5, 10]$  and (a) for  $F = 1.01$  and  $F = 1.03$  (b) for  $F = 1.05$  and  $F = 1.1$ .

frequency. Since the output capacitor  $C_o$  charges in each resonance cycle, to avoid the influence of  $v_o(t)$  on the estimation of tank resonance frequency, the frequency of the first full cycle is measured. Fig. 10 shows the impulse waveform across  $M_1$  and  $M_2$ , and the resonant inductor current measures a tank resonance frequency of  $98\text{kHz}$ . No significant change is observed in the value of tank resonance frequency, even when the experiment is repeated by shorting the secondary of the transformer. Assuming the influence of stray capacitance on the tank resonance frequency is negligible,  $L_{reff}$  is computed from the measured tank resonance frequency by choosing  $C_{reff} = C_r = 16\text{nF}$ , as given in Table II. The  $L_{reff}$  is computed as,

$$L_{reff} = \frac{1}{4\pi^2 C_r f_r^2} = 164.8\mu\text{H} \quad (28)$$

Hence the SRC designed for the experiment will have characteristic impedance of,

$$Z_c = \sqrt{L_{reff}/C_r} = 101.4\Omega \quad (29)$$

Using the SRC parameters given in Table II, the reflected resistance to the primary of the transformer having turns ratio

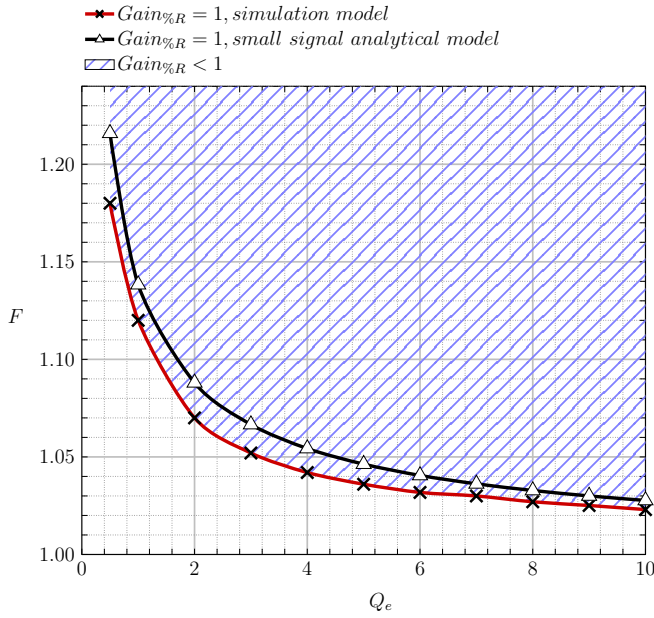


Fig. 8. Curve in the  $F$  versus  $Q_e$  plain for which audiosusceptibility gain is unity. For the region above the curve  $Gain\%R$  is less than unity. The curves from the small signal model and simulation are compared.

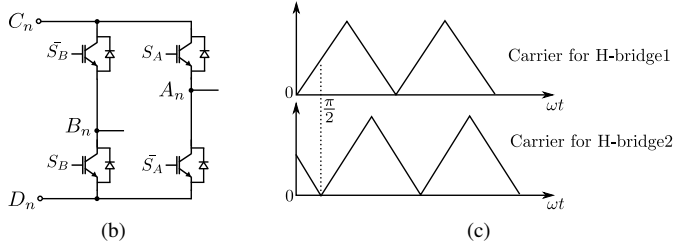
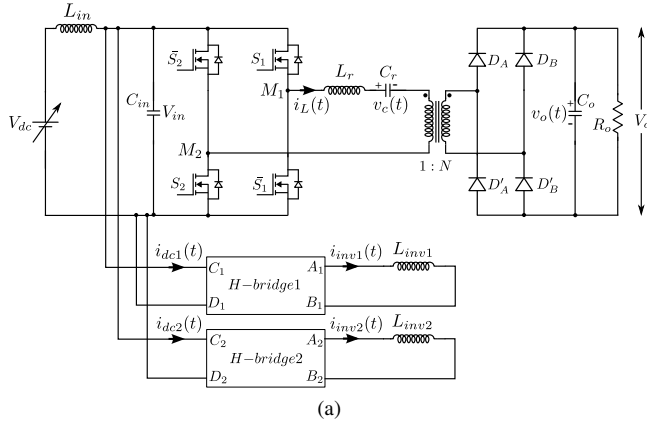


Fig. 9. (a) Test circuit to evaluate the audiosusceptibility of SRC (b) schematic of H-bridge (c) carrier for H-bridge1 and H-bridge2.

$1 : N$  is given by (30) [14].

$$R_{ac} = \frac{8}{\pi^2} \frac{R_o}{N^2} = 31.66\Omega \quad (30)$$

Therefore, effective quality factor of SRC is given by,

$$Q_e = \frac{Z_c}{R_{ac}} = 3.2 \quad (31)$$

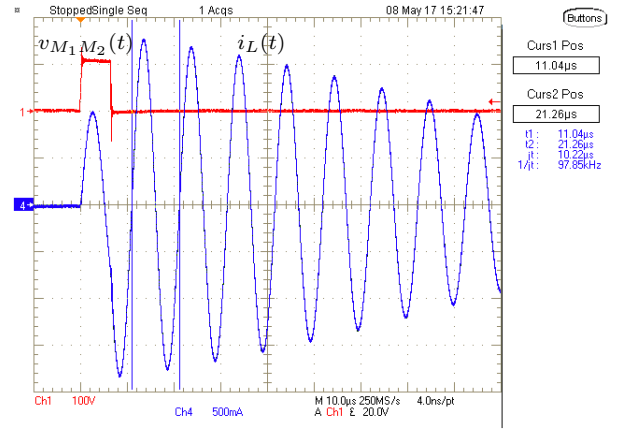


Fig. 10. Experimental measurement with output load shows the impulse voltage  $v_{M_1M_2}(t)$  and  $i_L(t)$ . SRC tank resonance frequency measured from  $i_L(t)$  is also shown.

TABLE III  
VARIOUS PARAMETERS OF SRC THAT IS USED IN THE EXPERIMENT

Parameters	Values
Effective resonant inductor, $L_{reff}$	164.8 $\mu H$
Effective resonant capacitor, $C_{reff}$	16nF
Characteristic impedance, $Z_c$	101.4 $\Omega$
Reflected resistance to the primary, $R_{ac}$	31.66 $\Omega$
Effective quality factor, $Q_e$	3.2
Resonance frequency, $f_r$	98kHz
Ratio of switching to SRC tank resonance frequency, $F$	1.01

For the experimental evaluation of audiosusceptibility, the  $F$  value is chosen as 1.01. Various derived characteristics of SRC are summarized in Table III.

### C. Audiosusceptibility experimental results

The input dc voltage applied for the experiment is 8.4V results in an output voltage of 133.5V. This gives a dc gain of 15.9. The input ripple frequency in  $V_{in}$  is varied from 100Hz to 4kHz. From the measured magnitude of input and output ripple and the obtained dc gain, by (25) the audiosusceptibility gain is computed at each frequency. Fig. 11 shows the experimentally obtained audiosusceptibility gain with the dc input ripple frequency. AS resonance is observed in Fig. 11 at frequency 1550Hz. Substituting the parameters given in Table III into (24), the AS resonance frequency for input ripple is obtained analytically as 1570Hz.

The magnitude spectrum of the input ripple and output ripple obtained from experiment at input ripple frequency of 1550Hz which corresponds to the AS resonance frequency is shown in Fig. 12. The rms values of output and input ripple measured are 1.182V and 23mV respectively, gives a gain of 34.2dB. The time domain input and output ripple recorded from the experiment for the frequency of 1550Hz is shown in Fig. 13. Fig. 11 also shows that beyond 2114Hz the gain offered by SRC to input ripple is less than unity as the gain



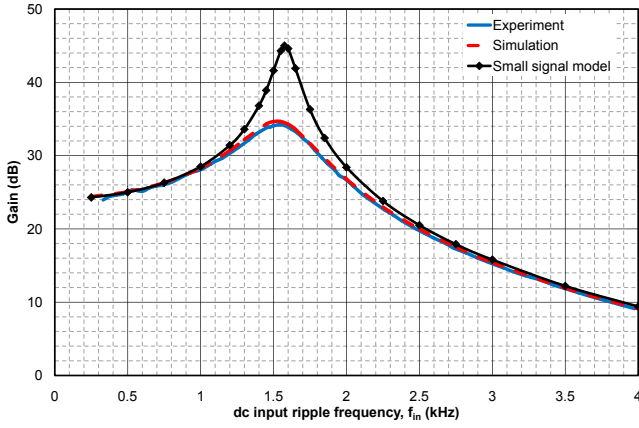


Fig. 11. Comparison of audiosusceptibility gain from experiment, simulation and small signal model of SRC.

at  $2114\text{Hz}$  is  $23\text{dB}$  which is equal to the turns ratio of the transformer.

Various SRC component values given in Table II are used in the simulation to find the audiosusceptibility gain for various values of input ripple frequency. Similarly the audiosusceptibility gain is computed with the small signal audiosusceptibility model derived in (23). The audiosusceptibility gain plot obtained from experiment, simulation and small signal model are compared in Fig. 11. The audiosusceptibility gain at resonance condition obtained from experiment, simulation and small signal model are  $34.2\text{dB}$ ,  $34.6\text{dB}$  and  $44\text{dB}$  respectively. The frequency at which maximum audiosusceptibility gain occurred in experiment, simulation and small signal model is found to be closely matching and the values are  $1550\text{Hz}$ ,  $1550\text{Hz}$  and  $1570\text{Hz}$  respectively. From Fig. 11 the gain contributed by the small signal model is higher than that obtained from experiment and simulation. The audiosusceptibility small signal model is derived without considering the circuit elements such as the stray capacitance of the transformer,  $C_s$ , winding resistance and transformer magnetizing inductance.

TABLE IV

AUDIOSUSCEPTIBILITY RESONANCE FREQUENCY AND THE GAIN AT RESONANCE CONDITION OBTAINED FROM EXPERIMENT, SIMULATION WITH AND WITHOUT  $C_s$  AND SMALL SIGNAL MODEL

Parameters	Experiment	Simulation		AS Small signal model
		with $C_s$	with $C_s=0$	
AS gain at resonance (dB)	34.2	34.6	41.0	44.0
AS resonance frequency (Hz)	1550	1550	1575	1570

To verify this condition, the simulations are repeated by keeping the stray capacitance of the transformer to zero value. The audiosusceptibility gain obtained by experiment, simulation with  $C_s=0$  and small signal model are compared in Fig. 14. Fig. 14 shows that the audiosusceptibility gain with

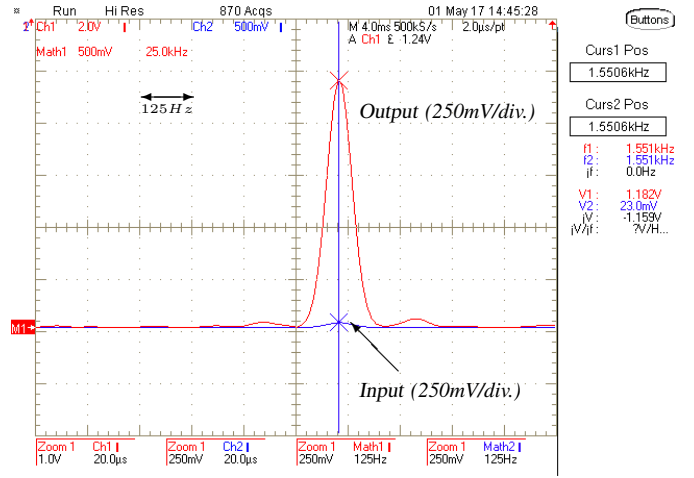


Fig. 12. Magnitude spectrum of input (Math2) and output (Math1) ripple corresponds to a frequency of  $1551\text{Hz}$ .

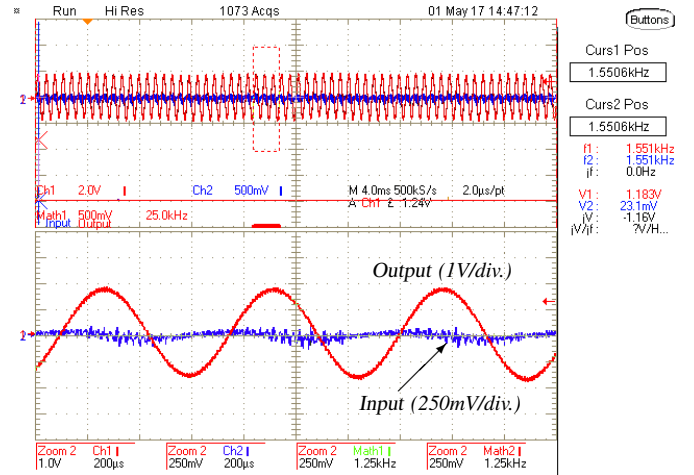


Fig. 13. AC coupled input (CH2) and output (CH1) ripple in time domain corresponds to a frequency of  $1551\text{Hz}$ .

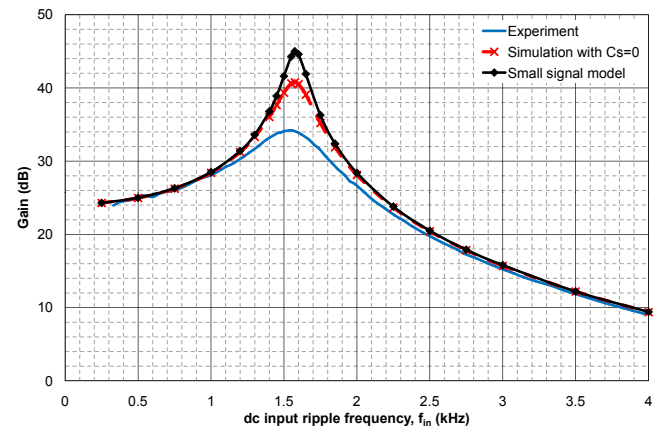


Fig. 14. Comparison of audiosusceptibility gain from experiment, simulation with  $C_s = 0$  and small signal model of SRC.

simulation, keeping the stray capacitance of the transformer

to zero, is close to the audiosusceptibility gain plot from the small signal model. Values for audiosusceptibility resonance frequency and the gain at resonance condition obtained from experiment, simulation with and without  $C_s$  and small signal model are tabulated in Table IV. The gain obtained from small signal model is close to gain from simulation with  $C_s=0$ . Also by introducing  $C_s$  in the simulation, the gain obtained from simulation is close to the experimental results. This shows that the small signal model is valid considering that it is formulated after neglecting parasitic elements. All results from the experiment are closely matching with the analytical results derived in section III.

## VI. CONCLUSION

The paper formulates a method to handle the 3 state variables of an SRC while obtaining state space model using exact discretization modelling approach. From the non-linear state space model a small signal state space model is derived.

Considering practically observed assumptions, the small signal model is simplified and the audiosusceptibility transfer function is derived. The analysis of AS transfer function shown a possibility of resonance peak and an expression relating the AS resonance frequency for input ripple with different SRC components is derived. The frequency response of AS transfer function is verified by simulation and compared with the derived analytical expressions for different values of  $Q_e$  and  $F$ . From further analysis a region is identified that connects  $Q_e$  and  $F$  with the “less than unity gain” audiosusceptibility gain. The obtained region is verified by time domain simulation results and such region helps in the design of SRC converters with superior audiosusceptibility performance. A test setup for the experimental evaluation of AS transfer function is also proposed in the paper. The influence of stray parameters on AS characteristics is discussed. All the analysis on analytical model, simulation and experimental results on a  $10kW$  SRC are found to be closely matching.

## APPENDIX

The elements of the matrices  $A_d$  and  $B_d$  are given in (A.1) and (A.2) respectively. The elements of  $T_d$  is given in (A.3) where as elements of  $T_{kx}$  and  $T_{ku}$  are given in (A.4).

$$\begin{aligned} \mathbf{a}_{11} &= \cos \omega_r T_s, \quad \mathbf{a}_{12} = -\frac{\sin \omega_r T_s}{Z_c}, \quad \mathbf{a}_{21} = Z_c \sin \omega_r T_s, \quad \mathbf{a}_{22} = \cos \omega_r T_s, \quad \mathbf{a}_{13} = \frac{\sin \omega_r T_s + 2 \sin \omega_r (T_s - T_3) - 2 \sin \omega_r (T_s - T_1)}{N Z_c}, \\ \mathbf{a}_{23} &= \frac{1 - \cos \omega_r T_s - 2 \cos \omega_r (T_s - T_3) + 2 \cos \omega_r (T_s - T_1)}{N}, \quad \mathbf{b}_{11} = \frac{\sin \omega_r T_s - 2 \sin \omega_r \frac{T_s}{2}}{Z_c}, \quad \mathbf{b}_{21} = 2 \cos \omega_r \frac{T_s}{2} - \cos \omega_r T_s - 1 \end{aligned}$$

where  $\omega_r = 1/\sqrt{L_r C_r}$ ,  $Z_c = \sqrt{L_r/C_r}$

(A.1)

$$\begin{aligned} \mathbf{a}_{31} &= G_1 \left[ 2e^{\frac{T_1}{R_o C_o}} g_1'(T_1) - 2e^{\frac{T_3}{R_o C_o}} g_1'(T_3) + e^{\frac{T_s}{R_o C_o}} g_1'(T_s) - \frac{1}{R_o C_o} \right] \\ \mathbf{a}_{32} &= \frac{G_1}{Z_c} \left[ 2e^{\frac{T_3}{R_o C_o}} g_1(T_3) - 2e^{\frac{T_1}{R_o C_o}} g_1(T_1) - e^{\frac{T_s}{R_o C_o}} g_1(T_s) - \omega_r \right] \\ \mathbf{a}_{33} &= -e^{\frac{T_s}{R_o C_o}} + \frac{G_1}{N Z_c} \left[ 2e^{\frac{T_1}{R_o C_o}} g_1(T_1) - 2e^{\frac{T_3}{R_o C_o}} g_1(T_3) + e^{\frac{T_s}{R_o C_o}} g_1(T_s) + \omega_r + 4e^{\frac{T_3}{R_o C_o}} g_1(T_3 - T_1) \right. \\ &\quad \left. - 2e^{\frac{T_s}{R_o C_o}} g_1(T_s - T_1) + 2\omega_r e^{\frac{T_1}{R_o C_o}} + 2e^{\frac{T_s}{R_o C_o}} g_1(T_s - T_3) + 2\omega_r e^{\frac{T_3}{R_o C_o}} \right] \\ \mathbf{b}_{31} &= \frac{G_1}{Z_c} \left[ 2e^{\frac{T_1}{R_o C_o}} g_1(T_1) - 2e^{\frac{T_3}{R_o C_o}} g_1(T_3) + e^{\frac{T_s}{R_o C_o}} g_1(T_s) + \omega_r + 4e^{\frac{T_3}{R_o C_o}} g_1(T_3 - \frac{T_s}{2}) - 2e^{\frac{T_s}{R_o C_o}} g_1(\frac{T_s}{2}) + 2\omega_r e^{\frac{T_s/2}{R_o C_o}} \right] \end{aligned}$$

where  $g_1(\cdot) = \frac{1}{R_o C_o} \sin \omega_r(\cdot) - \omega_r \cos \omega_r(\cdot)$ ,  $g_1'(\cdot) = \frac{dg_1(\cdot)}{d\omega_r(\cdot)}$ ,  $G_1 = -\frac{1}{N C_o} e^{-\frac{T_s}{R_o C_o}} \frac{1}{\left(\frac{1}{R_o C_o}\right)^2 + \omega_r^2}$

(A.2)

$$\begin{aligned} \mathbf{td}_{11} &= \frac{2\omega_r V_o \cos \omega_r (T_s - T_1)}{N Z_c}, \quad \mathbf{td}_{12} = -\frac{2\omega_r V_o \cos \omega_r (T_s - T_3)}{N Z_c}, \quad \mathbf{td}_{21} = \frac{2\omega_r V_o \sin \omega_r (T_s - T_1)}{N}, \quad \mathbf{td}_{22} = -\frac{2\omega_r V_o \sin \omega_r (T_s - T_3)}{N} \\ \mathbf{td}_{31} &= -\frac{2I_L \cos \omega_r T_1}{N C_o} e^{-\frac{(T_s - T_1)}{R_o C_o}} + \frac{2V_c \sin \omega_r T_1}{N Z_c C_o} e^{-\frac{(T_s - T_1)}{R_o C_o}} + \frac{G V_o}{N Z_c} \left[ 2G_2 e^{\frac{T_1}{R_o C_o}} \sin \omega_r T_1 - 4\omega_r e^{\frac{T_3}{R_o C_o}} g_1'(T_3 - T_1) + \right. \\ &\quad \left. 2\omega_r e^{\frac{T_s}{R_o C_o}} g_1'(T_s - T_1) + \frac{2\omega_r}{R_o C_o} e^{\frac{T_1}{R_o C_o}} \right] - \frac{2V_{in} \sin \omega_r T_1}{N Z_c C_o} e^{-\frac{(T_s - T_1)}{R_o C_o}} \end{aligned}$$

$$\mathbf{td}_{32} = \frac{2I_L \cos \omega_r T_3}{N C_o} e^{-\frac{(T_s - T_3)}{R_o C_o}} - \frac{2V_c \sin \omega_r T_3}{N Z_c C_o} e^{-\frac{(T_s - T_3)}{R_o C_o}} + \frac{G V_o e^{\frac{T_3}{R_o C_o}}}{N Z_c} \left[ -2G_2 \sin \omega_r T_3 + \frac{2\omega_r}{R_o C_o} + 4G_2 \sin \omega_r (T_3 - T_1) - 2\omega_r e^{\frac{(T_s - T_3)}{R_o C_o}} g'_1 (T_s - T_3) \right] + \frac{G V_{in} e^{\frac{T_3}{R_o C_o}}}{Z_c} \left[ -2G_2 \sin \omega_r T_3 + \frac{4g_2 (T_3 - \frac{T_s}{2})}{R_o C_o} - 4\omega_r g'_2 (T_3 - \frac{T_s}{2}) \right]$$

$$\text{where } g_2(\cdot) = \frac{1}{R_o C_o} \sin \omega_r(\cdot) + \omega_r \cos \omega_r(\cdot), \quad g'_2(\cdot) = \frac{dg_2(\cdot)}{d\omega_r(\cdot)}, \quad G_2 = \left( \frac{1}{R_o C_o} \right)^2 + \omega_r^2$$

(A.3)

$$\begin{aligned} \mathbf{tx}_{11} &= \frac{\cos \omega_r T_1}{f'_{T1}}, \quad \mathbf{tx}_{12} = -\frac{\sin \omega_r T_1}{Z_c f'_{T1}}, \quad \mathbf{tx}_{13} = \frac{\sin \omega_r T_1}{N Z_c f'_{T1}}, \quad \mathbf{tx}_{21} = \frac{\cos \omega_r T_3}{f'_{T3}} + \frac{2V_o \omega_r \cos \omega_r (T_3 - T_1) \cos \omega_r T_1}{N Z_c f'_{T1} f'_{T3}} \\ \mathbf{tx}_{22} &= -\frac{\sin \omega_r T_3}{Z_c f'_{T3}} - \frac{2V_o \omega_r \cos \omega_r (T_3 - T_1) \sin \omega_r T_1}{N Z_c^2 f'_{T1} f'_{T3}}, \quad \mathbf{tx}_{23} = \frac{\sin \omega_r T_3 - 2 \sin \omega_r (T_3 - T_1)}{N Z_c f'_{T3}} + \frac{2V_o \omega_r \cos \omega_r (T_3 - T_1) \sin \omega_r T_1}{N^2 Z_c^2 f'_{T1} f'_{T3}} \\ \mathbf{tu}_{11} &= \frac{\sin \omega_r T_1}{Z_c f'_{T1}}, \quad \mathbf{tu}_{21} = \frac{\sin \omega_r T_3 - 2 \sin \omega_r (T_3 - \frac{T_s}{2})}{Z_c f'_{T3}} + \frac{2V_o \omega_r \cos \omega_r (T_3 - T_1) \sin \omega_r T_1}{N Z_c^2 f'_{T1} f'_{T3}} \end{aligned}$$

$$\text{where } f'_{T1} = -\frac{f_{T1}}{dT_1}, \quad f'_{T3} = -\frac{f_{T3}}{dT_3}$$

(A.4)

## ACKNOWLEDGMENT

This work is supported by Ministry of Electronics and Information Technology, Govt. of India, through NaMPET programme.

## REFERENCES

- [1] S. D. Johnson, A. F. Witulski, and R. W. Erickson, "Comparison of resonant topologies in high-voltage dc applications," *IEEE Trans. Aerosp. Electron. Syst.*, vol. 24, no. 3, pp. 263–274, May, 1988.
- [2] N. Vishwanathan and V. Ramanarayanan, "High voltage dc power supply topology for pulsed load applications with converter switching synchronized to load pulses," in *Proc. 5th Int. Conf. Power Electronics and Drive Systems (PEDS)*, Singapore, Nov. 2003, pp. 618 – 623.
- [3] D. Maksimovic and R. Zane, "Small-signal discrete-time modeling of digitally controlled PWM converters," *IEEE Trans. Power Electron.*, vol. 22, no. 6, pp. 2552–2556, Nov., 2007.
- [4] R. Middlebrook and S. Cuk, "A general unified approach to modelling switching power converter stages," in *Proc. IEEE Power Electronics Specialists Conf.*, Cleveland, Ohio, Jun. 1976, pp. 18–34.
- [5] V. Vorperian, "High-Q approximation in the small signal analysis of resonant converters," in *Proc. IEEE Power Electronics Specialists Conf.*, Toulouse, France, Jun. 1985, pp. 707–715.
- [6] R. King and T. Stuart, "Small-signal model for the series resonant converter," *IEEE Trans. Aerosp. Electron. Syst.*, vol. AES-21, no. 3, pp. 301–319, May, 1985.
- [7] V. Vorperian and S. Cuk, "Small-signal analysis of resonant converters," in *Proc. IEEE Power Electronics Specialists Conf.*, Albuquerque, New Mexico, Jun. 1983, pp. 269–282.
- [8] J. Sun and H. Grotstollen, "Averaged modeling and analysis of resonant converters," in *Proc. IEEE Power Electronics Specialists Conf.*, Seattle, Jun. 1993, pp. 707–713.
- [9] E. Yang, F. Lee, and M. Jovanovic, "Small-signal modeling of series and parallel resonant converters," in *Proc. IEEE Applied Power Electronics Conf.*, Boston, Feb. 1992, pp. 785–792.
- [10] S. Tian, F. Lee, and Q. Li, "A simplified equivalent circuit model of series resonant converter," *IEEE Trans. Power Electron.*, vol. 31, no. 5, pp. 3922–3931, May, 2016.
- [11] A. R. Brown and R. D. Middlebrook, "Sampled-data modeling of switching regulators," in *Proc. IEEE Power Electronics Specialists Conf.*, Boulder, Colorado, Jul. 1981, pp. 349–369.
- [12] J. Stahl, H. Steuer, and T. Duerbaum, "Discrete modeling of resonant converters-Steady state and small signal description," in *Proc. IEEE Energy Conversion Congress and Expo. (ECCE)*, Raleigh, Sept. 2012, pp. 1578–1584.
- [13] T. G. Subhash Joshi and V. John, "Small Signal Audio Susceptibility Model for Series Resonant Converter," in *IEEE Int. Conf. on Power Electronics, Drives and Energy Systems (PEDES)*, Trivandrum, Dec. 2016, pp. 1–6.
- [14] R. W. Erickson and D. Maksimovic, *Fundamentals of Power Electronics*, 2nd ed. Kluwer Academic Publishers, 2004, pp.713-716.
- [15] M. E. Elbuluk, G. C. Verghese, and J. G. Kassakian, "Sampled-data modeling and digital control of resonant converters," *IEEE Trans. Power Electron.*, vol. 3, no. 3, pp. 344–354, Jul., 1988.